Energy transport along Fermi-Pasta-Ulam chains containing binary isotopic disorder: Zero-temperature systems

K. A. Snyder
Building and Fire Research Laboratory, National Institute of Standards and Technology, Gaithersburg, Maryland 20899-8615, USA

T. R. Kirkpatrick
Institute for Physical Science and Technology and Department of Physics, University of Maryland, College Park, Maryland 20742, USA
(Received 9 March 2006; published 21 April 2006)

Energy transport in binary isotopically disordered (BID) Fermi-Pasta-Ulam chains is characterized by dissipation from harmonic energy eigenstates. Using a continuum analog for the corresponding harmonic portion of the Hamiltonian, the time-independent wave amplitude is calculated for a plane wave that is incident upon the disorder and the solution is mapped onto the discrete chain. Anderson localization causes the initial energy to be localized near the incident end of the chain, and in the absence of anharmonicity the wave amplitude is stationary in time. For sufficient anharmonicity, however, mode transitions lead to dissipation. Energy transport along the chain is quantified using both the second moment of the site energy and the number of masses contributing to transport, estimated from the localization parameter. Over the time scales studied, the second moment of the site energy increased linearly in time, yielding an effective transport coefficient. At low and intermediate impurity concentrations, the transport coefficient can be characterized by a competition between impurity scattering and diffusion over a distance comparable to the localization length. At the highest concentrations, the localization parameter indicates that there is significant mode transition suppression in BID systems and the transport coefficient is proportional to the initial localization length. This result suggests that vibrational energy transitions in strongly localized modes retain the spatial extent of the interacting modes.

DOI: 10.1103/PhysRevB.73.134204 PACS number(s): 71.23.−k, 63.20.Pw, 45.05.+x

I. INTRODUCTION

Nonlinear binary disordered chains are useful systems for studying the essential characteristics of energy dissipation and transport in materials. Although binary disorder is an idealized model, it has practical applications to a number of fields: isotopic disorder effects and linewidth broadening in spectroscopy.[1–3] The glass transition has been considered in terms of binary changes in elasticity parameters,[4] and isolated mechanical defects can lead to a variety of nonlinear effects.[5,6]

An interesting behavior of binary isotopic disorder (BID) occurs in discrete lattices, where the system undergoes a pure-disordered-pure transition as the impurity concentration varies from 0 to 1. For harmonic one-dimensional chains composed of discrete elements, finite disorder destroys spatial invariance and gives rise to Anderson[7] localization, characterized by spatially localized eigenstates.

We are interested in the rate of localized energy dissipation along a discrete nonlinear chain. Previous studies have used either a singular (one or very few elements) pulse or a Gaussian envelope for the initial displacement.[8–12] Because neither is an eigenstate of the system, both will begin to propagate ballistically and will exhibit some measure of dissipation in both anharmonic and harmonic systems. In time, scattering and localization slow the rates of propagation and dispersion.

To eliminate the initial ballistic motion, the initial displacement is an energy eigenstate of the corresponding harmonic chain, and it remains localized until mode transitions occur. For the harmonic chain, the wave remains localized indefinitely, and there is no energy transport. The addition of anharmonicity will give rise to mode transitions that will delocalize the wave and lead to energy transport through the chain. Instead of having a ballistic-diffusive transition, this initial condition leads to a localized-diffusive transition.

The question of whether Fermi-Pasta-Ulam (FPU) chains have anomalous thermal conductivity (a function of system length) by virtue of momentum conservation remains an active area of interest.[13–18] It should be noted that discussions of this topic[13,17] have been limited to FPU chains without isotopic disorder. Some of the first studies of disordered systems, using either isotopic disorder[19] or spring constant disorder,[20] were inconclusive as to whether the thermal conductivity was a function of length. Recent studies of thermal conductivity in disordered FPU chains have shown normal heat conduction in long systems close to zero temperature.[21] This result is consistent with the argument that Fourier's law is satisfied when there are both phonon-phonon and phonon-lattice interactions.[14]

To study energy transport, the following numerical experiment will use the binary disordered Fermi-Pasta-Ulam[22] chain with quartic spring potentials (FPU-β). Starting from the initial harmonic energy eigenstate, numerical integration will be used to calculate the spatial distribution of energy as a function of time. Based on a local concept of thermal transport,[4] an effective transport coefficient will be calculated[23] from the second moment of the site energy, and the method is compared to the Helfand[24] moments for thermal conductivity. The second moment will exhibit diffusive behavior, a fact that will be corroborated qualitatively using the localization parameter[25,26] to calculate the number of

masses over which the total energy is distributed.

The effective transport coefficient will be studied as a function of impurity concentration. The mode transfer behavior will change as the concentration varies from dilute (a wavelength far smaller than the mean free path) to very dense (a wavelength spanning many impurities). Energy transfer in dilute systems will be characterized by impurity scattering. As the impurity concentration increases, transport becomes dominated by interacting localized modes.[27,28] For systems having the greatest impurity concentration, energy transfer will occur among strongly localized modes. As a result, the spatial extent of these interacting modes will persist and the original localization length will remain the dominant length scale over which transport occurs.

II. NUMERICAL EXPERIMENT

A. FPU-β chain

The FPU-β chain is composed of masses interacting with nearest neighbors through springs. The Hamiltonian H of a chain having N masses is a function of the mass momenta p_i and the mass displacements q_i about their equilibrium position:

$$H = \sum_i^N \frac{p_i^2}{2m_i} + \frac{K}{2}(q_i - q_{i-1})^2 + \frac{\beta}{4}(q_i - q_{i-1})^4. \tag{1}$$

The harmonic spring force coefficient K is set equal to 1, and in the absence of impurities, each mass has the same value $m_0=1$. The site energy E_i is the sum of the kinetic energy plus one-half of the neighboring spring potential energies. The total energy E_T is the sum of the site energies. In this experiment, the displacement at each end is fixed at zero.

Whenever possible, the results are expressed in dimensionless units through the use of appropriate scaling factors. Time is scaled by the natural frequency ω_0 of a single-harmonic oscillator:

$$\omega_0 = \left(\frac{K}{m_0}\right)^{1/2}. \tag{2}$$

Lengths are scaled by the equilibrium mass separation distance a.

The time-dependent behavior was determined by numerical integration using the sixth-order Yoshida[29] symplectic integration algorithm. Specifically, the best results were obtained from the "solution A" coefficients (see Table 1 in Ref. 29). For the systems studied here, the time step Δt was approximately 1/200 the period of the initial mode. This time step was consistent with that used elsewhere[8,30] and was chosen as a compromise between speed and accuracy, and the results were insensitive to twofold changes in Δt. Using this time step, the energy fluctuations were always less then 0.2% (see the Appendix).

B. Semi-infinite approximation

In most cases, very-low-frequency waves will propagate down the chain and reach the far end. If the wave is reflected, it could affect the accuracy of the transport calculation. To mitigate this effect, 10% of the masses at the far end were given a viscous force F_{vis}:

$$F_{vis} = -\eta\dot{q}. \tag{3}$$

This approach has been used elsewhere to achieve a similar effect.[31] For these calculations, a viscosity η of 0.2 was sufficient to eliminate the effects of reflection.

The viscous damping, combined with the accurate time integration, simplified the task of identifying finite-size effects. As the system length decreased and the localization length increased, the likelihood of a considerable amount of energy reaching the far end of the system increased. Fortunately, this occurrence was easily identified by changes in the system total energy.

C. Initial displacement

The initial condition was a stationary state exhibiting Anderson localization for the harmonic component of the Hamiltonian. This initial condition was chosen so that for $\beta=0$ there is no net energy transport and these systems could be used as a test to confirm the accuracy of the model and the numerical integration.

The continuum Kronig-Penney liquid model[32,33] is used to estimate the initial displacement. For the harmonic FPU chain, the analogous continuum system is an elastic rod having mass density $\mu=m_0/a$ and Youngs modulus $Y=Ka$. Between the impurities, a longitudinal displacement wave $\psi(x,t|\omega)$ with frequency ω will propagate with phase velocity $v_p=\sqrt{Y/\mu}$. A harmonic oscillator impurity, approximated by a point defect, located at x' will give rise to a reactive force that is proportional to the impurity impedance $Z(\omega)$ (Ref. 34):

$$\left[\mu\frac{\partial^2}{\partial t^2} - Y\frac{\partial^2}{\partial x^2} = -Z(\omega)\delta(x-x')\frac{\partial}{\partial t}\right]\psi(x,t|\omega). \tag{4}$$

For a harmonic system, one can assume a sinusoidal solution with frequency ω [$\psi=\phi(x|\omega)e^{-i\omega t}$]:

$$\left[\frac{\partial^2}{\partial x^2} + \zeta^2 = \frac{-i\omega}{Y}Z(\omega)\delta(x-x')\right]\phi(x|\omega), \tag{5}$$

where $\zeta=\omega/v_p$.

Equation (5) is solved for a system having impurities at integer locations with probability c. The boundary conditions are a unit amplitude incident wave and a reflected wave at one end and only a transmitted wave at the other end. The initial displacement for the FPU system is taken from the real component of the solution $\phi(x|\omega)$.

D. Impurity cross section

To put some of the results in a familiar context, it will be useful to characterize an impurity by its cross section to the original wave. The cross section σ of an individual impurity can be expressed as a function of the impurity impedance Z (Ref. 34):

$$\sigma = \frac{|Z(\omega)|^2}{|Z(\omega)|^2 + 4Km_0}. \tag{6}$$

Here, the isotopic impurities consist of a constant mass m_+ added to the existing mass m_0; m_+ may be either positive or negative, and the impurity mass m_I is (m_0+m_+). It has been determined that for a discrete system, the impedance Z of a mass impurity in a continuum system[34] must be modified by c_s, which is the ratio of the group velocity $(v_g=\partial\omega/\partial k)$ to the phase velocity v_p (Ref. 35):

$$Z(\omega) = -\mathrm{i}\omega m_+/c_s. \tag{7}$$

For the discrete chain, $c_s=\cos(ka/2)$, where k is the wave number $(2\pi/\lambda)$ and λ is the displacement wavelength.

E. Continuum-discrete mapping

The boundary condition for the chain is zero displacement at each end. Because the continuum solution $\phi(x=0,L|\omega)$ will (with almost certainty) not equal zero at $(x=0,L)$, the continuum solution was truncated to accommodate the constraints of zero displacement at both ends. The continuum solution is first mapped onto the discrete chain with no modification, and then, starting at one end and moving along the chain, the end is relocated to the mass having the smallest oscillation amplitude, and its displacement is fixed at zero. The process is repeated at the opposite end of the chain.

For this experiment, a nominal displacement (equal to an integer multiple of the unit spacing) is chosen first. The working wavelength is the nominal wavelength minus $0.2a$. With this wavelength, the displacement amplitudes repeat every five wavelengths, with nine nodal points occurring at different fractions of the spacing a. Probabilistically, this reduces the minimum-mass oscillation amplitude by nearly an order of magnitude over an integer wavelength.

An example input displacement is shown in Fig. 1 for a system with length 10 000, displacement wavelength 31.8, impurity cross section 0.5, and impurity concentration 0.01. The small dots in the figure represent the initial displacement of the masses. The larger solid circles denote the location and displacement of the impurities. The effect of the impurities is to change both the displacement amplitude and the phase. Also shown in the figure is a dashed line that is proportional to $e^{-(i-x_0)/\xi}$, where x_0 is the location of the first impurity and ξ is the localization length (to be discussed subsequently). Although this particular initial condition suggests that the initial displacement amplitudes decrease monotonically, that is not always the case.

F. Dense systems

For BID systems, the localization length is not a monotonic function of impurity concentration. Rather, the localization length has a minimum with respect to impurity concentration; at higher concentrations, the system returns to a "pure" system. The localization length ξ of BID systems at dilute impurity concentrations, such that $c\lambda \ll 1$, can be calculated from the resistivity scaling law[36]

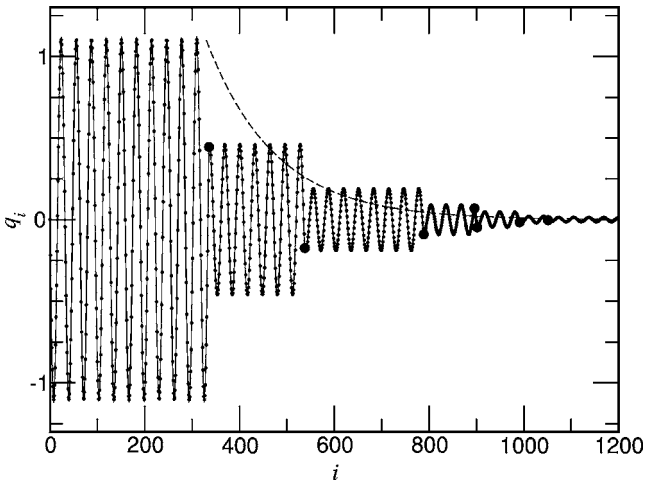

FIG. 1. Initial displacements q_i for a particular system having wavelength 31.8, impurity concentration 0.01, and impurity scattering cross section 0.5. Mass displacements are denoted by small circles, and the impurity locations are denoted by large circles. The first impurity is located at $x_0=336$, and the dashed line is proportional to $e^{-(i-x_0)/\xi}$.

$$\xi_{c\to 0}^{-1} = c\,\ln(1+\rho). \tag{8}$$

The single-impurity resistivity ρ is related to the single-impurity cross section σ (Ref. 37):

$$\rho = \frac{\sigma}{1-\sigma}. \tag{9}$$

As the impurity concentration increases beyond a value of $\frac{1}{2}$, the system approaches a homogeneous system. In the limit $c\to 1$, the system is again ordered and the localization length diverges:

$$\xi_{c\to 1}^{-1} = (1-c)\ln(1+\rho'). \tag{10}$$

The quantity ρ' characterizes a system having an equilibrium mass (m_0+m_+), an impurity mass m_0, and oscillations at the same frequency ω (Ref. 35):

$$k' = \frac{2}{a}\sin^{-1}\left[\frac{\omega}{2}\sqrt{\frac{m_0+m_+}{K}}\right], \tag{11a}$$

$$c_s' = \cos(k'a/2), \tag{11b}$$

$$\rho' = \frac{(-m_+\omega/c_s')^2}{4K(m_0+m_+)}. \tag{11c}$$

The relation for k' in Eq. (11a) is an improvement over the low-frequency approximation given previously.[35] Because the localization length of a system is analogous to its conductivity and the systems described by $\xi_{c\to 0}$ and $\xi_{c\to 1}$ occur independently and in parallel, the localization length over all values of impurity concentration can, by analogy to electrical conductors, be approximated by a sum of the two:[35]

$$\xi = \xi_{c\to 0} + \xi_{c\to 1}. \tag{12}$$

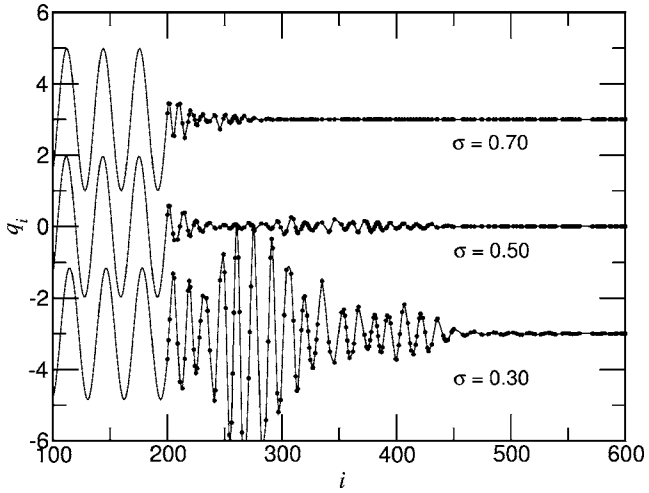

FIG. 2. Initial displacements q_i for systems having wavelength 31.8, impurity concentration 0.50, and all three impurity scattering cross sections. Mass displacements are denoted by line, and the impurity locations are denoted by circles. The systems were shifted horizontally so that the first impurity is located at $i=200$.

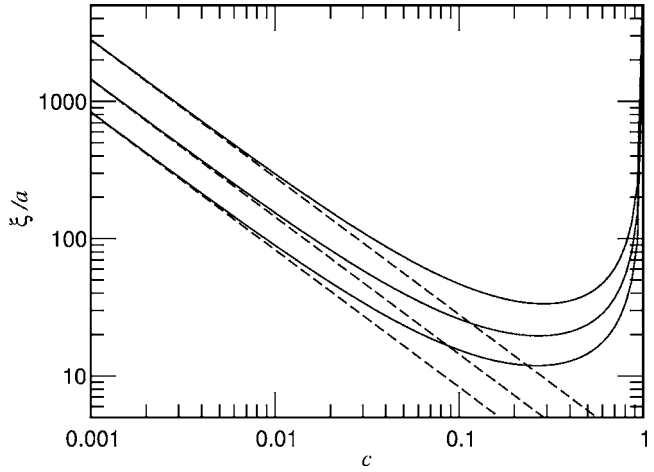

FIG. 3. Localization length ξ as a function of impurity concentration c for systems having displacement wavelength $\lambda=31.8$. The three solid curves, from upper to lower, are for $\sigma=0.30$, 0.50, and 0.70, respectively. The dashed lines are the dilute limit localization length $\xi_{c\to 0}$.

When the concentration of the impurities increases to $c\lambda>1$, the energy eigenstate becomes more complicated than the dilute impurity example shown in Fig. 1. Example initial conditions for the highest impurity concentration considered in this experiment ($c=0.5$) are shown in Fig. 2 for three scattering cross sections. At these high concentrations, although the frequency remains constant everywhere, the wave structure in the disordered region is considerably more complex than that shown in Fig. 1 for a dilute system.

G. Parameter space

For the nonlinear systems considered, the incident wave had wavelength $\lambda=31.8$ and anharmonicity parameter $\beta=1$. For all the systems from which energy transport was measured, the added mass m_+ had one of three values: 6.605, 10.089, and 15.412. With respect to the wavelength $\lambda=31.8$, these impurity masses had scattering cross sections 0.30, 0.50, and 0.70, respectively.

The primary experimental parameter was the impurity concentration c. The impurity-concentration lower limit was constrained by computing resources. A previous study of these systems revealed that approximately 32 impurities are required in a chain to ensure reliable ensemble statistics.[35] The upper concentration limit was 0.5. Above this concentration, the behavior is analogous to a study of the system having mass m_I and impurity mass m_0.

The initial displacement was a localized mode with localization length ξ. To better understand the length scale over which the energy was initially distributed, the aforementioned impurity masses are used to calculate the localization length, using Eq. (12), for a wave having displacement 31.8, and the results are shown in Fig. 3. The dilute-limit result $\xi_{c\to 0}$ is shown as a dashed line and begins to depart from ξ at concentrations for which $c\lambda\approx 1$.

Figure 3 also reveals the utility of choosing a nominal displacement wavelength $\lambda=32$. For $c\lambda>1$, the addition of impurities has a nonlinear effect on localization length. Naturally, one would like to see whether this nonlinear behavior has any effect on energy transport. For shorter displacement wavelengths, the deviation between ξ and $\xi_{c\to 0}$ would not occur until proportionately higher impurity concentrations. Alternatively, using a longer wavelength would reduce the rate of mode transitions considerably, requiring excessively long computational times.

III. THERMAL CONDUCTION

For systems at zero temperature, there are no formal methods (e.g., thermostatted systems,[19] Green-Kubo,[38] or NEMD[38,39]) for uniquely determining the thermal conductivity. Rather, other similar experiments at zero temperature have used pulse propagation rate and the second moment of the site energy[8–12] to characterize an effective transport coefficient. Here, the second moment of the site energy is used and its relationship to Helfand moments[24] is discussed.

The Helfand moments can be used to calculate the thermal conductivity of a collection of freely moving particles in thermal equilibrium. The energy fluctuation $\tilde{E}_i$ for the ith particle is the difference between the instantaneous site energy E_i and the ensemble-averaged value $\langle E_i\rangle$:

$$\tilde{E}=E_i-\langle E_i\rangle. \tag{13}$$

If the energy fluctuation is conserved and the energy flux has a linear dependence on $\nabla\tilde{E}$, the quantity $\tilde{E}_i(x,t)$ will satisfy the diffusion equation. For the boundary conditions that the initial value $\tilde{E}_i(x,0)$ is localized about x_{i0} and that $\tilde{E}_i(\pm\infty,t)=0$, the solution for $\tilde{E}_i(x,t)$ is Gaussian and the measure of spatial extent is the second moment of $\tilde{E}_i$:

$$2\kappa t\tilde{E}_i(x,0)\sim\int(x-x_{i0})^2\tilde{E}(x,t)dx, \tag{14}$$

where κ is the thermal conductivity.

As $\tilde{E}_i$ represents the fluctuation for a single particle, a bulk expression requires an ensemble integral of the second moment. Making no assumption about the independence of particle energies, the thermal conductivity can be calculated from a double sum over particle positions:[24]

$$H^p = \left\langle \sum_{i,j} (x_i - x_{j0})^2 \tilde{E}_i(x,t) \tilde{E}_j(x,0) \right\rangle \sim 2\kappa t. \qquad (15)$$

Replacing conservation of momentum with conservation of energy yields an equivalent alternative expression[24]

$$H^e = \left\langle \left[\sum_i (x_i \tilde{E}_i - x_{i0} \tilde{E}_{i0}) \right]^2 \right\rangle \sim 2\kappa t. \qquad (16)$$

Equations (15) and (16) are the Helfand moments for calculating the thermal conductivity of a bath of particles.

There are a number of differences between fluctuations in a bath of particles and energy propagation along a discrete chain. Equations (15) and (16) characterize a bath of freely moving particles. By contrast, in the FPU chain energy moves, but the masses are, more or less, stationary. This is not entirely problematic, however, because one can still evaluate the energy that is at x_i, and the problem can be changed to one in which the energy is evaluated at points along the chain.

Another important distinction is that Eqs. (15) and (16) are functions of the energy fluctuations in an equilibrated system at temperature T. By contrast, a pulse moving through an FPU chain is a system that is not in equilibrium and the portion of the chain farthest from the initial disturbance is initially at zero temperature. In principle, after very long times, the chain would eventually reach equilibrium, with the energy distributed over all the masses. Because the conceptual problem of interest is a semi-infinite chain, the equilibrium energy $\langle E_i \rangle$ would approach zero. Under the assumption $\langle E_i \rangle = 0$, the fluctuation energy $\tilde{E}$ of the bath problem becomes the site energy E_i of the nonequilibrium chain problem.

By analogy to Eqs. (15) and (16), the energy transport in the FPU-β chain will be characterized by the second moment of the energy. Assuming that the initial pulse occupies a small portion of the entire system, a useful measure is the second moment about zero:

$$\frac{\sum_i r_i^2 E_i}{\sum E_i} \sim 2Gt. \qquad (17)$$

The position $r_i = ia$ is the equilibrium location of the ith mass. The quantity G is an effective transport coefficient that is neither self-diffusion nor thermal conductivity. To eliminate the effects of fluctuations, the initial value is subtracted from the subsequent values. In addition, the equation is generalized to allow for arbitrary powers of E_i:

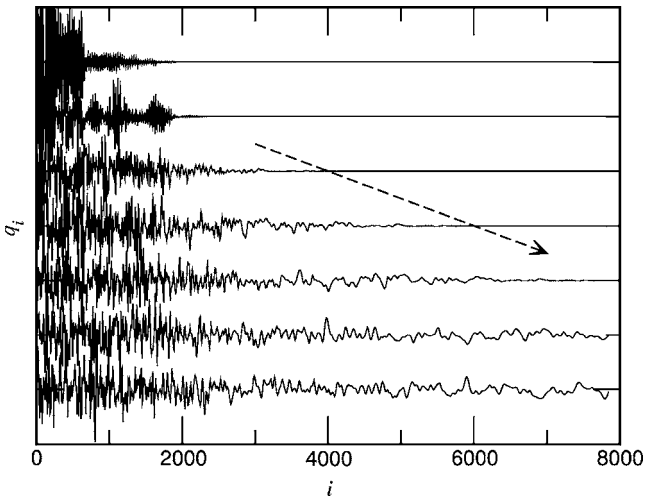

FIG. 4. Wave displacement q_i along a chain at various times. Chain length is 8000, added mass m_+ is 10.089, and impurity concentration is 0.010. Each curve represents a time difference of 2000 and is offset by a value of one for demonstration purposes. Dashed arrow denotes ballistic propagation.

$$M_n(t) = \left\langle \frac{\sum_i r_i^2 E_i^n}{\sum E_i^n} - M_n(0) \right\rangle \sim 2G_n t. \qquad (18)$$

These definitions are similar to those used by Fröhlich *et al.*[40] and are consistent with the local concept of thermal transport of Wagner *et al.*[4]

A comparison among M_1, M_2, H^p, and H^e is made from the early response of a system of length 8000 that is initially in a localized mode. The wavelength is 31.8, the impurity mass is 11.089, the impurity concentration is 0.010, and $\beta = 1$. The displacement q along the system is shown in Fig. 4 at time intervals of $\omega_0 \Delta t = 2000$. (The curves are offset vertically from one another, by a distance a, for comparison purposes.) The data in the figure show that long-wavelength displacements move virtually ballistically along the chain (parallel to dashed arrow) while the higher-frequency displacements propagate a considerably shorter distance over the same time interval.

At regular time intervals, M_1 and M_2 are calculated, along with H^p and H^e (assuming that $\tilde{E} = E_i$ and $\langle E_i \rangle = 0$). The results of the calculations are shown in Fig. 5. All values are normalized by the initial localization length ($\xi \approx 155$). H^p and H^e are also normalized by the total energy E_T to be on the same scale as M_1 and M_2. The two pairs of equations, (M_1, H^p) and (M_2, H^e), generally agree with one another, but M_1 and M_2 are greater in value than the corresponding H^p and H^e. At the shortest times, M_1 and H^p give the nearly the same value.

H^p and H^e are equivalent descriptions of thermal conductivity. Therefore, the difference between H^p and H^e for the case of an initially localized pulse demonstrates that thermal conductivity for these systems is not well defined. As a result, the second moments M_n characterize some effective, yet undefined, transport coefficient.

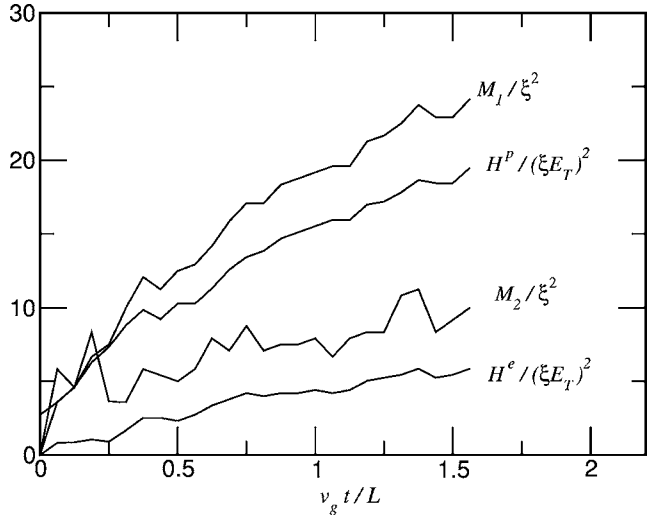

FIG. 5. Moments M_1, M_2, H^p, and H^e as a function of time for the system shown in Fig. 4. Quantities are normalized, using localization length ξ and total energy E_T, to make the values dimensionless.

These curves are also instructive in pointing out the distinction between pulse propagation and energy propagation. From Fig. 4 it is clear that low-frequency waves propagate nearly ballistically through these systems, starting from $t \approx 0$. By contrast, Fig. 5 shows no ballistic behavior, suggesting that the vast majority of the energy is in the higher-frequency modes located within the initially localized region. Moreover, the moments shown in Fig. 5 all continue to increase after there has been sufficient time for the low-frequency ballistic modes to reach the far end of the chain.

IV. EQUIPARTITION

The dynamics of both mode transitions and spatial energy equipartition will influence the response of the systems. A previous experiment to study the mode transition rate for similar chains configured as small hoops initially excited in a single-wave-number eigenmode suggested that impurities initially hasten the decay of energy in the excited mode.[41] Over long times, however, the rate diminished because the energy became localized at the impurities. Because the impurities were heavier than the background, the oscillations at the impurities were smaller, reducing the rate of mode transitions because of the quadratic dependence of amplitude.

The systems studied here, however, have energy initially localized at one end, with the energy already localized at the impurities. Once transitions start to occur, the new modes, which are not localized over the same length scale, will propagate and both spontaneously decay and scatter from impurities.

A. Localization parameter

As the mode transitions occur, the energy will propagate along the chain, redistributing the energy. As the energy becomes more evenly distributed among the masses, the energy becomes less localized. A measure of how uniformly the energy is distributed among N masses is the localization parameter Γ (Refs. 25 and 26:

$$\Gamma = N\left\langle \frac{\sum^N E_i^2}{\left(\sum^N E_i\right)^2} \right\rangle. \tag{19}$$

The value of Γ is a minimum for ergodic behavior and increases as the degree of localization increases.

The localization parameter can be used to estimate the number of masses over which energy is distributed. The maximum value of Γ is N, when all the energy is localized at one mass. At long time, Γ approaches a constant, $\Gamma_\infty = \Gamma(t \to \infty)$, which only depends on the value of β.[42] For the FPU-β system, with $\beta = 1$, the equilibrium value Γ_∞ is approximately 1.8. Thus, Γ_∞/Γ is approximately equal to the fraction of the chain over which energy is distributed.

B. Participating modes

Another useful measure of ergodicity is the number of harmonic modes contributing to the energy located at a particular mass. The systems to be studied are initially excited in one mode (in frequency space). The time required for the system to excite the maximum number of modes should correspond to the time required for the system to become ergodic.

The energy in a particular mode E_ω is estimated from the harmonic approximation involving the Fourier-transformed (FT) displacement $Q_i(\omega)$ and momentum $P_i(\omega)$ of mass m_i:

$$E_{i,\omega} = \frac{1}{2}\left(m_i \omega^2 Q_i^2 + \frac{P_i^2}{m_i} \right). \tag{20}$$

The energy is then normalized using the total number of frequency modes, N_ω, considered in the FT:

$$e_{i,\omega} = \frac{E_{i,\omega}}{\frac{N_\omega}{\sum_\omega E_{i,\omega}}}. \tag{21}$$

These normalized energies are a measure of energy entropy S_i at mass m_i (Refs. 25, 30, 43, and 44):

$$S_i = -\sum_\omega e_{i,\omega} \ln(e_{i,\omega}). \tag{22}$$

If all the energy is in a single-frequency mode, S equals 0. If the energy is distributed evenly among all frequency modes, S equals $\ln N_\omega$.

An alternative expression for the energy entropy is $\exp(S)$. This is the equivalent number of modes contributing to the overall entropy if the energy is uniformly distributed among those modes. To make comparisons among results using different values for N_ω, results are expressed as the fraction of possible modes $n_\omega(i)$ at mass m_i:

$$n_\omega(i) = \frac{\exp(S_i)}{N_\omega}. \tag{23}$$

The fraction of participating modes along a section of chain is determined by calculating $n_\omega(i)$ for some of the masses within the section of interest and then reporting the average value n_ω.

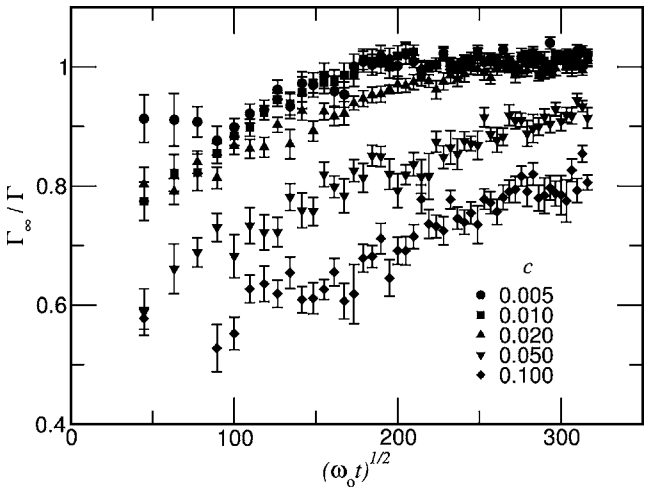

FIG. 6. Localization parameter Γ as a function of time t for a periodic system with length 636, initial wavelength 31.8, impurity cross section 0.5, and anharmonicity 1.0.

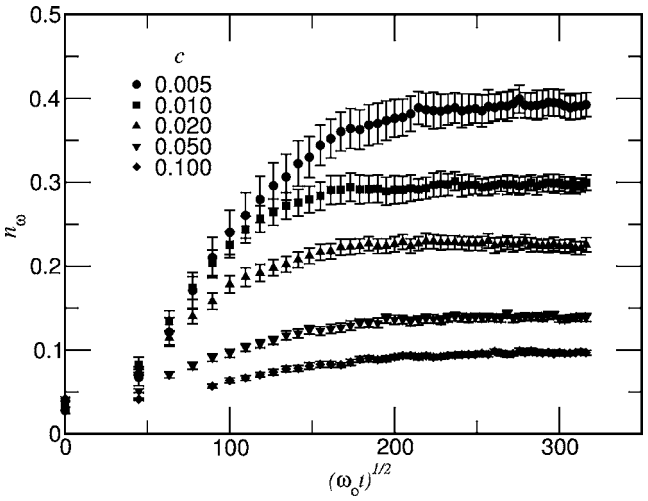

FIG. 7. Fraction of participating modes n_ω as a function of time t for a periodic system with length 636, initial wavelength 31.8, impurity cross section 0.5, and anharmonicity 1.0.

C. Hoop example

The localization parameter Γ and the fraction of participating modes n_ω were developed to study systems in which the energy is initially distributed throughout. For the systems studied here, the initial energy is intentionally localized at one end of the system. If such a system was divided into two equal halves, the initial values for Γ and n_ω in one half would be very different from the values calculated for the other half of the system. Nonetheless, the parameters do have utility for these systems.

One application is the study of behavior within a short section of chain. If the section of chain is quasilocalized (very few modes are present, oscillating with nearly constant amplitude), mode transitions are the primary mechanism for inducing energy transport. A hoop (periodic boundary conditions), initially excited in one-wave-number mode, could be used to study the behavior of a similar section within a much longer section that is itself quasilocalized. The time-dependent behavior of the localization parameter Γ and the relative number of participating modes n_ω would characterize the energy redistribution, with respect to both space and mode frequency.

A brief numerical calculation of Γ and n_ω is made to study the effect of impurity concentration on mode transitions. The initial condition is a BID hoop having length 636, wavelength 31.8, and $\beta=1$ (single-k mode). This initial condition differs from an Anderson localized state (single-ω mode). In a disordered system, a single-k mode will excite multiple-ω modes, accelerating the initial rate of mode transitions. Nevertheless, the results illuminate general behavior for nonlinear BID systems.

The effects of impurity concentration on the spatial distribution of energy and on the mode transition rate are shown in Figs. 6 and 7. The energy distribution data in Fig. 6 show that the time for energy to become distributed among all the masses is relatively constant in systems for which $c\lambda < 1$. At higher concentrations, after a delay, the initial rate of energy redistribution is nearly the same as for the dilute systems, but the fraction of the system involved is much less. This suggests that at concentrations for which $c\lambda > 1$, the energy redistribution among masses behaves differently from dilute systems in a fundamental way.

This assessment is consistent with the data shown in Fig. 7 for the fraction of participating modes, n_ω. The rate that new modes are produced in dilute systems is a constant, until n_ω approaches its asymptotic value. At concentrations for which $c\lambda > 1$, however, the initial rate of mode production does not reach the dilute system initial rate. Therefore, although the rate that the energy is distributed among masses is the same for dilute and concentrated systems, the rate of mode production is much slower in concentrated systems.

The decreasing asymptotic value for n_ω with increasing impurity concentration indicates that modes are suppressed significantly in concentrated systems. This is consistent with the effect of impurities on the spectral density u of BID systems. The presence of impurities forces zeros in $u(\omega)$,[45,46] thereby constraining mode transitions. Moreover, as the impurity concentration increases, the spectral density in the interval $[4K/m_I \leqslant \omega^2 \leqslant 4K/m_0]$ (assuming $m_I > m_0$) becomes increasingly suppressed, eventually containing isolated δ functions.[47–49] If the frequency of the initial displacement is in the interval $[0 \leqslant \omega^2 \leqslant 4K/m_I]$, that mode will be in a continuous portion of $u(\omega)$ for all values of impurity concentration. As the impurity concentration increases, the range of frequencies in the accessible portion of u decreases, thus suppressing more of the higher-frequency modes. Although low-frequency ($\omega \ll \omega_0$) mode generation will not be effected, it has already been demonstrated that these modes have no measurable effect on bulk energy transport. Therefore, in concentrated systems, new modes of any significance will likely have a frequency in proximity to the initial frequency.

V. RESULTS

Some of the results to be presented include estimates of uncertainty for quantities calculated from ensemble averages.

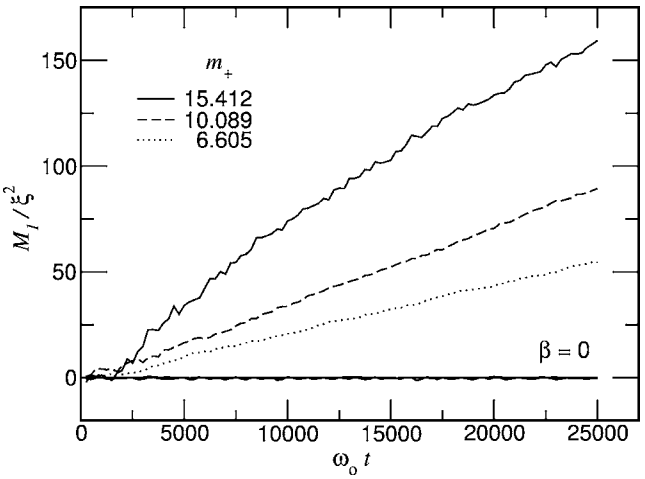

FIG. 8. The ratio M_1/ξ^2 as a function of time for the systems having impurity concentration 0.500 and length 16 000. The $\beta=1$ data have positive slopes, and all the $\beta=0$ data fall on top of one another.

For a calculation performed on an ensemble of W systems, there is a population standard deviation s and an average value. For this study, the average value is the meaningful quantity. The uncertainty in the reported average value is $s/\sqrt{W}$ and is referred to here as the standard deviation in the mean (SDM). All error bars appearing in figures represent the SDM, unless explicitly stated otherwise.

There are two special cases within the parameter space that require special consideration. The M_n data for the nonlinear systems are only meaningful when the M_n data for the corresponding harmonic system is a constant. This is true for all systems, especially at concentrations for which $c\lambda \gg 1$. In theory, M_n for harmonic systems would be a constant for all time. In practice, the mapping of the continuum system onto the discrete lattice and the relocation of the ends introduced a small amount of instability that led to small fluctuations in M_n. These fluctuations, however, were far smaller than the changes that can occur in the anharmonic systems.

As a brief example, Fig. 8 is a plot of M_1 as a function of time for systems having impurity concentration 0.5 and length 16 000. In the figure, the $\beta=1$ data appear as lines having positive slope. The harmonic $\beta=0$ data for all three impurity masses lie upon one another near $M_1=0$. Figure 8 is doubly instructive. It demonstrates that the oscillations for the $\beta=0$ data are negligible, even for systems for which the second moment has the smallest value. Moreover, the harmonic data remain stable in concentrated systems: $c\lambda \gg 1$.

A. Time exponent

A quantitative characterization of M_n is made by assuming a power-law dependence on time t:

$$M_n = 2G_n t^{\delta_n}. \tag{24}$$

The first task is to determine the value of the exponent δ_n so as to distinguish among ballistic, diffusive, or subdiffusive, transport. The calculation of δ_n is affected by initial transients, and the details of the analysis are given in the Appendix. The time intervals used to calculate δ_n were constrained by the initial transients at small times and total energy conservation at long times. The specific intervals are shown in Table I for each system length.

TABLE I. Interval from which δ_n was calculated for systems having length L.

L	Interval
16000	$5000 < \omega_0 t < 20000$
32000	$10000 < \omega_0 t < 25000$
64000	$20000 < \omega_0 t < 50000$
96000	$20000 < \omega_0 t < 80000$

The results of the analyses for δ_1 are summarized in Fig. 9 for all the systems. (In the figure, the symbols at a particular concentration are displaced horizontally to distinguish individual error bars representing the SDM.) With only one exception, the estimated values for δ_1 are within one SDM of 1. Therefore, the subsequent analysis of M_1 is based on a linear model with respect to time.

The results of the analysis for δ_2 were not conclusive for these systems. Although the values of δ_2 were near 1 for most systems, there was considerably more variability than for δ_1. Moreover, it was difficult to establish a precise value for δ_2 at higher concentrations. As a result, the subsequent analysis is confined to M_1.

B. Transport coefficient

Based on the results for δ_1, estimates for $2G_1$ were based on the assumption of a linear relationship between M_1 and t over the same intervals shown in Table I. Although M_1 was determined by linear regression, calculating the uncertainty in M_1 required a slightly more involved analysis; details are give in the Appendix.

Estimates of $2G_1$ for all the systems considered are plotted in Fig. 10 as a function of the impurity concentration c.

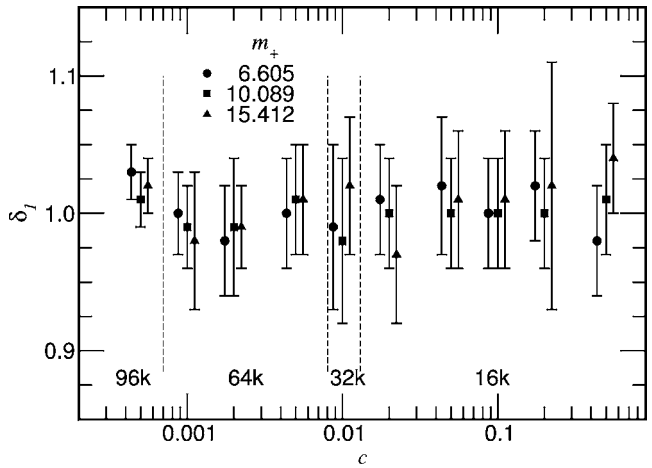

FIG. 9. The time exponent δ_1 for G_1 as a function of impurity concentration c for impurity cross sections $\sigma=0.30$, 0.50, 0.70. Numbers between vertical dashed lines denote N ($k=1000$).

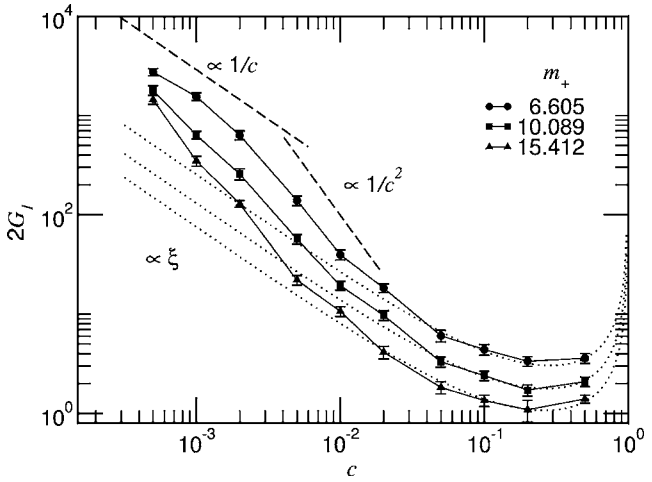

FIG. 10. Transport coefficient G_1 as a function of impurity concentration c for impurity cross sections $\sigma=0.30$, 0.50, 0.70. Dotted lines are proportional to $\xi(\sigma)$.

The calculated values appear as solid symbols having error bars that represent the SDM. The solid lines connecting the symbols are only to guide the eye. The two dashed line segments appearing above the data indicate slopes that are proportional to $1/c$ and $1/c^2$.

Data for $2G_1$ in Fig. 10 exhibit different behavior in three regions. At the lowest concentrations, $2G_1$ is proportional to c^{-1} for the two smaller impurity masses. At higher concentration, the coefficient $2G_1$ is proportional to c^{-2} for all three impurity masses. This transition is not apparent in the results of Payton *et al.*[19] on a similar system having thermostats because their computing resources prevented them from resolving the smaller concentrations required to see the effect.

The interesting behavior occurred at the highest concentrations. For all three impurity masses, the transport coefficient is proportional to the initial localization length ξ. This effect was also observed by Payton *et al.*,[19] but was not discussed in the context of a localization length. The three dotted curves labeled $\propto\xi$ are proportional to the localization lengths that appear in Fig. 3 for $\lambda=31.8$. The value of ξ for each impurity mass is multiplied by the same coefficient (approximately 0.09) to make the curves best agree with the measured transport coefficient.

C. Localization parameter

The localization parameter can also be used as a measure of energy propagation. Although systems of different lengths were used, energy transport, starting from a localized state, should be independent of total system length. Based on the previous discussion of the localization parameter, the ratio L/Γ is proportional to the number of masses over which the total energy is distributed. For a given m_I and c, and assuming that $L \gg \xi$, the number of masses over which energy is distributed should be independent of total system length. Therefore, the ratio L/Γ will serve as a means for comparing results from systems of different lengths.

If the linear time dependence of the second moment M_1 indicates diffusive behavior, the number of masses involved in energy transport should increase in proportion to $t^{1/2}$. In addition, because transport in dilute systems is proportional to c^{-1}, the quantity cL/Γ should approach a constant for systems with low impurity concentrations. The quantity cL/Γ, as a function of $t^{1/2}$, is plotted in Figs. 11–13 for most of the systems studied. In the figures, curves for smaller impurity concentration appear consecutively lower in the graph.

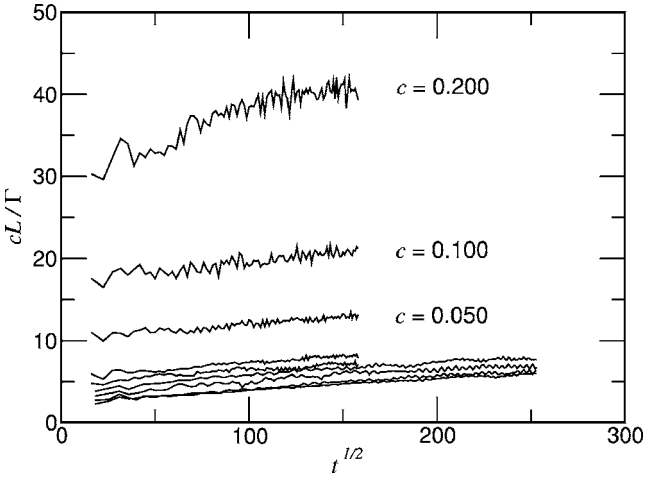

FIG. 11. Localization parameter Γ as a function of time $t^{1/2}$ for systems having $m_+=6.605$.

There are two noteworthy features in Figs. 11–13. The number of masses participating appears to be proportional to $t^{1/2}$ over the time intervals considered, particularly for the dilute impurity systems. This is consistent with the expectation of a diffusive energy transport coefficient G_1. Also, as expected, the curves for the most dilute impurity concentrations appear to converge to a single line, supporting the c^{-1} dependence for the number of masses participating in energy transport, even for the $m_+=15.412$ systems.

VI. DISCUSSION

A. Concentration dependence

The transition from $1/c$ to $1/c^2$ dependence in G_1 can be explained, in part, using arguments based on the relevant

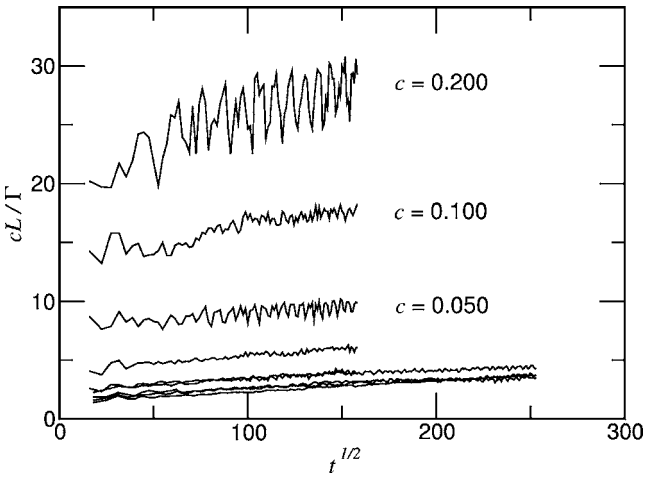

FIG. 12. Localization parameter Γ as a function of time $t^{1/2}$ for systems having $m_+=10.089$.

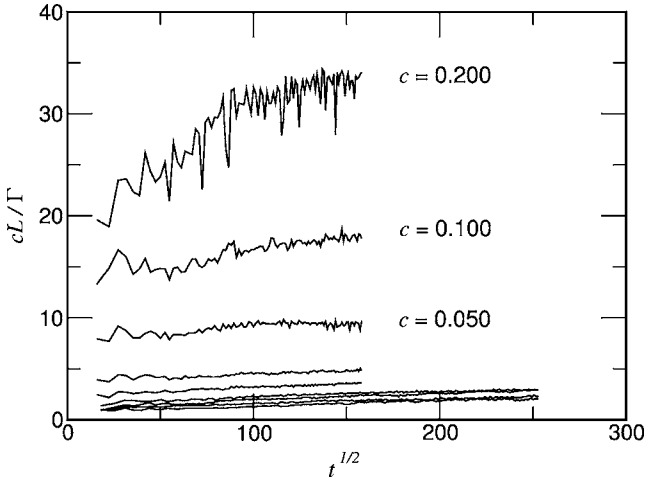

FIG. 13. Localization parameter Γ as a function of time $t^{1/2}$ for systems having $m_+=15.412$.

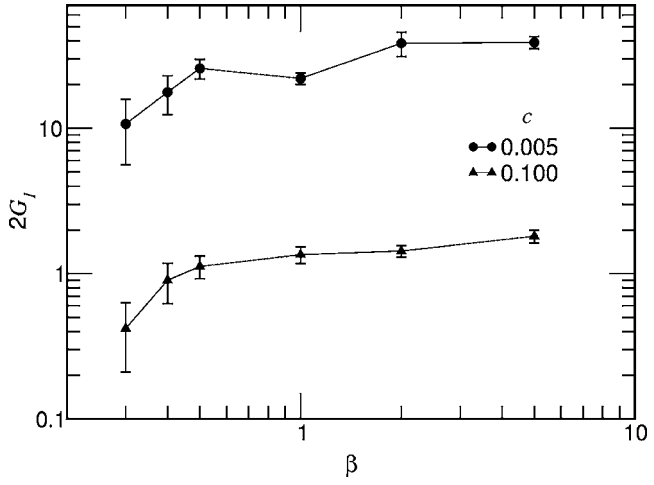

FIG. 14. Transport coefficient G_1 as a function of β for two impurity concentrations: $c=0.100$, 0.005, and $\sigma=0.70$.

length and time scales. At the lowest impurity concentrations, the chain is composed of long segments of homogeneous nonlinear chain between adjacent impurities. Scattering generates new modes that are not localized and begin to propagate ballistically along the chain. These waves will continue to propagate until they scatter from an impurity or undergo a spontaneous transition. A spontaneous transition along the homogeneous portion of the chain is unlikely to occur in the time required to span the distance between impurities. It is more likely that the impurities will initiate scattering. The time τ between these scattering events can be characterized by some relevant length scale Λ and the group velocity v_g:

$$\tau = \frac{\Lambda}{v_g}. \tag{25}$$

This scattering will give rise to an effective transport coefficient that is proportional to the group velocity:

$$G_1 \approx v_g \Lambda. \tag{26}$$

It is common to assume that the mean free path (MFP) $(c\sigma)^{-1}$ is the relevant length scale. In dilute-concentration BID systems, however, the localization length is slightly shorter than the mean free path. Regardless, the dissipation mechanism is a due to plane waves scattering over a length scale that is proportional to $1/c$ at low concentration.

As the impurity concentration increases, the localization length decreases and the wave experiences considerably more wave interference. As a result, transport is becoming dominated by interactions between and among localized modes.[27,28] The relevant time scale is the time t_ξ required for energy to diffuse a distance comparable to the localization length ξ:

$$G_1 \approx \frac{\xi^2}{t_\xi}. \tag{27}$$

For this type of behavior, the data in Fig. 10 show that the transport coefficient G_1 is proportional to $1/c^2$. Therefore, t_ξ is a weak function of concentration in this regime.

In the dense systems for which $c\lambda > 1$, the transport coefficient G_1 is proportional to ξ. For these concentrations, both G_1 and ξ are relatively weak functions of concentration. Moreover, the transport coefficient is proportional to the original localization length, and not some averaged value. Although energy transfer in these dense systems occurs from interactions among overlapping localized modes (as in the $G_1 \propto 1/c^2$ regime), the spatial extent of the interacting modes in strongly disordered systems persists for all subsequent interactions. As a result, the transport coefficient reflects this dependence on the initial spatial extent of the energy.

B. β dependence

The results given for $\beta=1$ are indicative of results for "large" values of β that are above the critical threshold that leads to ergodic behavior. As a check, the values of G_1 for two systems are calculated for different values of β. The two systems are $(c=0.005, \sigma=0.70)$ and $(c=0.100, \sigma=0.70)$, and the analysis for these systems was carried out in a manner identical to that for the $\beta=1$ data.

The values for G_1 are shown in Fig. 14 as a function of β. For $0.5 \leqslant \beta \leqslant 5.0$, the transport coefficient has a weak dependence on the anharmonicity. The transport coefficient decreased markedly as β fell below 0.5. This result is consistent with numerical experiments on finite-temperature nonlinear BID systems[19] and with numerical measurements for anharmonic silicon chains.[28] Therefore, although G increases slowly for β greater than 0.5, there does not appear to be any significance to any particular value for β that is greater than 0.5.

C. Time scale

The significance of the reported results presented depends, in part, on the relative duration of the calculation. One measure of duration, to gauge whether long times have been probed, is the ratio of the distance energy propagates along the system to its initial span. The maximum energy propagation length is proportional to $M_1(t_{max})$, and the initial span is

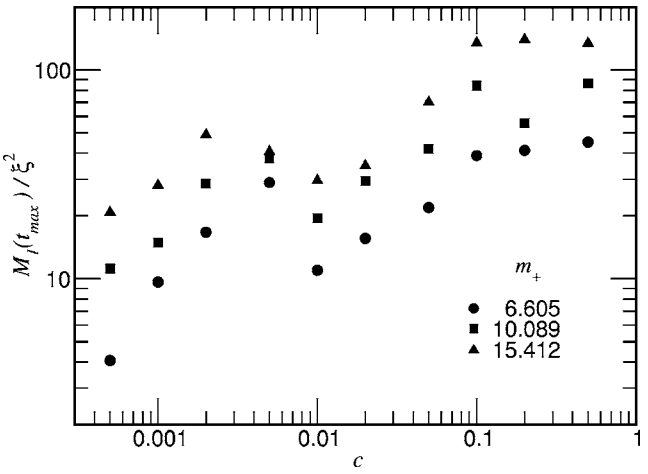

FIG. 15. The ratio $M_1(t_{max})/\xi^2$ as a function of impurity concentration c.

proportional to the initial localization length ξ.

The ratio $M_1(t_{max})/\xi^2$ for each system is plotted in Fig. 15. The ratio varied from 5 to 100, increasing with impurity concentration. The square root of this ratio is a measure of the depth to which energy propagated to the initial depth energy was distributed. Therefore, the energy penetration depth, relative the initial localization length, varied from 3 to 10.

VII. CONCLUSION

There is evidence for diffusive energy dissipation from energy eigenstates in binary isotopically disordered nonlinear FPU chains at zero temperature. Given sufficient anharmonicity, the second moment of the site energies increased linearly. Over the time scales studied, the square root of the second moment increased to a value that was approximately 10 times the initial localization length. The evidence for diffusive behavior was corroborated by the $t^{1/2}$ dependence for the number of masses over which energy was distributed, estimated from the localization parameter.

The most interesting aspect of the transport coefficient was the concentration dependence. At low impurity concentration c, the transport coefficient was proportional to c^{-1}. At higher impurity concentrations, the transport coefficient developed a c^{-2} dependence. This concentration dependence was consistent with a transition from transport dominated by impurity scattering to one in which interactions among overlapped localized modes dominating transport.

At the highest impurity concentrations, the concentration dependence of the transport coefficient was proportional to the original localization length. In strongly disordered systems for which $c\lambda > 1$, far fewer modes are produced, and at a slower rate. In addition, the character of the spectral density at these concentrations constrains mode production. The dynamics of the mode transition in combination with the fact that the localization length is a weak function of concentration for strongly disordered systems suggests that vibrational energy transfer among strongly localized modes yields new modes that retain the spatial extent of the interacting modes. As a result, the initial spatial extent of interacting modes is retained as the dominate length scale characterizing transport in strongly disordered binary isotopic systems.

ACKNOWLEDGMENTS

The authors would like to thank Jack Douglas of the Polymers Division (NIST) for his useful comments and discussion. This work was supported by the NSF under Grant No. DMR-01-32726 and by the National Institute of Standards and Technology (NIST) High Performance Construction Materials and Systems program in the Building and Fire Research Laboratory.

APPENDIX: DATA ANALYSIS

The analyses of the results involve some minor subtleties that deserve a clear exposition. Neglecting these subtleties and performing an ordinary least-squares (OLS) analysis of the data would lead to misleading results. Specifically, not adjusting for initial transient behavior would lead to a different conclusion regarding the existence of diffusive energy transport.

As mentioned previously, the reported uncertainties are the SDM calculated from the ensemble population standard deviation s. For an ensemble of W systems, the SDM reported here is $s/\sqrt{W}$. This uncertainty characterizes the reported average value from the population.

δ_1 analysis

The straightforward means of determining the time exponent $\delta_1 n$ is from the slope of a log-log plot of M_1 versus time t. This approach assumes that the power law dependence exhibits itself at $t=0$. In reality, there is a transient period, after which the value of M_1 begins to increase. Although this increase appears to be linear, the data must be corrected to eliminate the effect of the transient.

The effect of the transient behavior is negated by shifting the data for M_1 vertically. OLS linear regression is applied to the M_1 versus t data over the time intervals given in Table I. The intercept calculated from the OLS regression is subtracted from $M_1(t)$. The process is demonstrated in Fig. 16 for one particular system. The original M_1 data are shown as a solid line. Regression is applied to the interval [20 000, 50 000], and the data are shifted vertically (dashed line) so that the linear approximation to this interval has zero intercept. OLS linear regression is then applied to the logarithm of these adjusted data versus the logarithm of time. The slope of this regression calculation is the value reported in Fig. 9 for δ_1.

The uncertainty in δ_1 is calculated from both the regression residuals and the ensemble population of M_1 values. Fortunately, because the population standard deviation in M_1 increases in time, the logarithm transform yields uncertainties that are nearly constant over the time intervals of interest. The adjusted data from Fig. 16 are shown in Fig. 17, along with the ensemble population standard deviations that are denoted by horizontal error bars; the vertical risers are omitted for clarity. (The ensemble population standard devia-

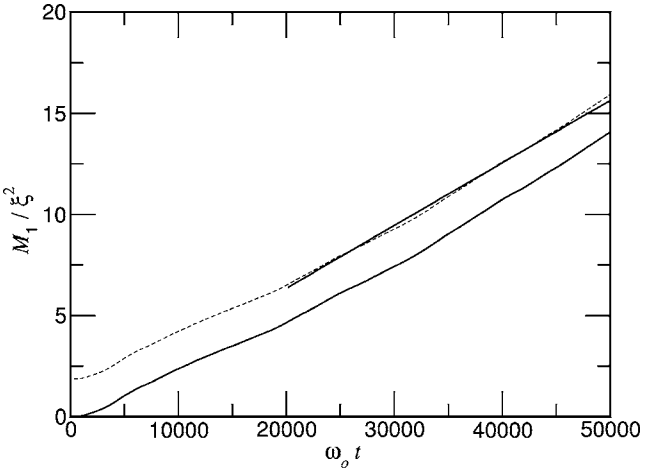

FIG. 16. M_1/ξ^2 as a function of time. System length is 64 000, impurity concentration is 0.002; single-impurity cross section is 0.30. The measured data appear as a solid line, the shifted data appear as dashed line, and the line segment denotes the range over which regression was performed.

tion, instead of the SDM, is shown in the figure for clarity of the demonstration. For an ensemble of W systems, the SDM error bars would be a factor of $\sqrt{W}$ smaller than those shown in the figure.) Also shown in the figure is the result of the regression analysis of the average values (solid straight line). The error bars denote the ensemble standard deviation s_{ens}, and the regression residuals represent the regression uncertainty s_{reg}.

The uncertainty in δ_1 is a function of both s_{ens} and s_{reg}. It is assumed that these two uncertainties are independent of one another and that they are additive. The uncertainty (estimated standard deviation) in the time exponent is

$$s_{\delta_1}^2 = \frac{s_{res}^2}{S_{XX}} + \frac{s_{ens}^2}{S_{XX}}. \tag{A1}$$

Because s_{ens} is the majority of s_{δ_1}, the uncertainty in $\delta_1(s_{\delta_1}/\sqrt{W})$ is referred to as a SDM and the coverage factor

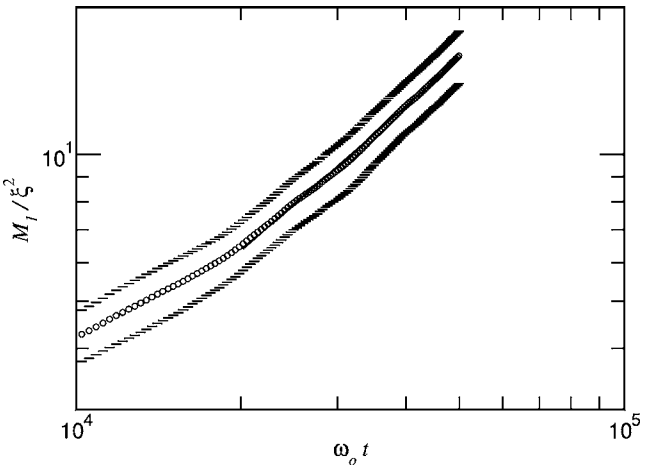

FIG. 17. A log-log plot of data in Fig. 16, along with horizontal error bars denoting the population standard deviation; the vertical risers are omitted for clarity. The solid line was determined by OLS regression applied to the mean values.

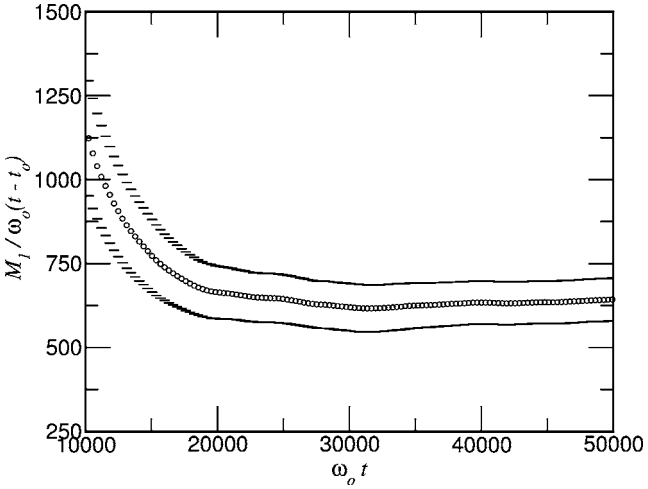

FIG. 18. Transformed M_1 to demonstrate how uncertainty in $2G_1$ is calculated. Horizontal lines denote error bars, and risers are omitted for clarity.

is approximately equivalent to one standard deviation for a normal distribution.

M_1 analysis

Based on the results of the δ_1 analysis, a hypothesis of a linear relationship between the second moment M_1 and time t cannot be rejected. The ability to use a linear model simplifies the analysis of M_1. The transport coefficient $2G_1$ is the slope that is calculated from OLS regression using a linear model.

The uncertainty in $2G_1$ cannot be determined from an OLS regression analysis of the M_1 versus t data because the uncertainties in M_1 increase in time. Fortunately, the data can be transformed into a more suitable format.

Assuming diffusive behavior, the values of M_1 are a collection of lines, radiating from the origin. The error model for the observations assumes that there exists an inherent error ϵ and that the total error increases linearly with time:

$$M_1(t_i) = A + 2G_1 t_i + t_i \epsilon_i. \tag{A2}$$

To use OLS techniques, the error term must be additive and constant. Equation (A2) can be transformed into a suitable model:

$$\frac{M_1(t_i)}{t_i} = \frac{A}{t_i} + 2G_1 + \epsilon_i. \tag{A3}$$

Unfortunately, the initial transient behavior that confounded the calculation of δ_1 must also be accounted for here. The error model assumes that the uncertainty grows linearly from $t=0$. In reality, the increase in M_1 occurred after some initial transient time t_0. To correct for this, linear regression is applied to the M_1 versus t data to determine the value of t_0. Using t_0, the data are shifted horizontally so that the linear region of interest has zero intercept. These shifted data are then transformed according to Eq. (A3).

The result of this transform, applied to both the mean and SDM, is shown in Fig. 18 for the data in Figs. 16 and 17. In Fig. 18, the error bars represent the SDM. Over the range of regression (see Table I), the SDM is relatively constant, consistent with Eq. (A3). Because the model in Eq. (A3) assumes a constant factor of $2G_1$, the error bars in Fig. 18 represent the SDM for $2G_1$. The reported uncertainty is the average width of the error bars over the regression interval.

[1] T. Held, I. Pfeiffer, and W. Kuhn, Phys. Rev. B **55**, 231 (1997).
[2] S. Rohmfeld, M. Hundhausen, L. Ley, N. Schulze, and G. Pensl, Phys. Rev. Lett. **86**, 826 (2001).
[3] F. Widulle, J. Serrano, and M. Cardona, Phys. Rev. B **65**, 075206 (2002).
[4] M. Wagner, G. Zavt, J. Vazquez-Marquez, A. Lütze, T. Mougios, G. Viliani, W. Frizzera, O. Pilla, and M. Montagna, Philos. Mag. B **65**, 273 (1992).
[5] I. Y. Solodov and B. A. Korshak, Phys. Rev. Lett. **88**, 014303 (2002).
[6] I. Solodov, J. Wackerl, K. Pfleiderer, and G. Busse, Appl. Phys. Lett. **84**, 5386 (2004).
[7] P. W. Anderson, Phys. Rev. **109**, 1492 (1958).
[8] R. Bourbonnais and R. Maynard, Phys. Rev. Lett. **64**, 1397 (1990).
[9] R. Bourbonnais and R. Maynard, Int. J. Mod. Phys. C **1**, 233 (1990).
[10] A. Sarmiento, R. Reigada, A. H. Romero, and K. Lindenberg, Phys. Rev. E **60**, 5317 (1999).
[11] H. Yamada and K. S. Ikeda, Phys. Rev. E **59**, 5214 (1999).
[12] A. Rosas and K. Lindenberg, Phys. Rev. E **69**, 016615 (2004).
[13] T. Prosen and D. K. Campbell, Phys. Rev. Lett. **84**, 2857 (2000).
[14] B. Hu, B. Li, and H. Zhao, Phys. Rev. E **57**, 2992 (1998).
[15] S. Lepri, R. Livi, and A. Politi, Physica D **119**, 140 (1998).
[16] S. Lepri, R. Livi, and A. Politi, Europhys. Lett. **43**, 271 (1998).
[17] T. Prosen and D. K. Campbell, Chaos **15**, 015117 (2005).
[18] S. Lepri, R. Livi, and A. Politi, Phys. Rev. Lett. **78**, 1896 (1997).
[19] D. N. Payton, M. Rich, and W. M. Visscher, Phys. Rev. **160**, 706 (1967).
[20] E. A. Jackson, J. R. Pasta, and J. F. Waters, J. Comput. Phys. **2**, 207 (1968).
[21] B. Li, H. Zhao, and B. Hu, Phys. Rev. Lett. **86**, 63 (2001).
[22] E. Fermi, J. Pasta, and S. Ulam (unpublished). See also *The Many-Body Problem*, edited by D. C. Mattis (World Scientific, Singapore, 1993), pp. 851–870.
[23] Technically speaking, the thermal conductivity as usually defined (as system size$\rightarrow\infty$) is zero. Here, we use the term "thermal conductivity" in a more general sense.
[24] E. Helfand, Phys. Rev. **119**, 1 (1960).
[25] T. Cretegny, T. Dauxois, S. Ruffo, and A. Torcini, Physica D **121**, 106 (1998).
[26] F. Piazza, S. Lepri, and R. Livi, J. Phys. A **34**, 9803 (2001).
[27] J. Fabian and P. B. Allen, Phys. Rev. Lett. **77**, 3839 (1997).
[28] D. M. Leitner, Phys. Rev. B **64**, 094201 (2001).
[29] H. Yoshida, Phys. Lett. A **150**, 262 (1990).
[30] R. Livi, M. Pettini, S. Ruffo, M. Sparpaglione, and A. Vulpiani, Phys. Rev. A **31**, 1039 (1985).
[31] R. Khomeriki, S. Lepri, and S. Ruffo, cond-mat/0407134 (unpublished.).
[32] R. de L. Kronig and W. G. Penney, Proc. R. Soc. London, Ser. A **130**, 499 (1931).
[33] J. M. Ziman, *Models of Disorder* (Cambridge University Press, Cambridge, England, 1979).
[34] P. M. Morse and K. U. Ingard, *Theoretical Acoustics* (Princeton University Press, Princeton, 1968).
[35] K. A. Snyder and T. R. Kirkpatrick, Phys. Rev. B **70**, 104201 (2004).
[36] P. W. Anderson, D. J. Thouless, E. Abrahams, and D. S. Fisher, Phys. Rev. B **22**, 3519 (1980).
[37] R. Landauer, Philos. Mag. **21**, 863 (1970).
[38] D. J. Evans and G. P. Morriss, *Statistical Mechanics of Nonequilibrium Liquids* (Academic Press, London, 1990).
[39] D. J. Evans, Phys. Lett. **91A**, 457 (1982).
[40] J. Fröhlich, T. Spencer, and C. E. Wayne, J. Stat. Phys. **42**, 247 (1986).
[41] K. A. Snyder and T. R. Kirkpatrick, Ann. Phys. **8**, SI 241 (1999).
[42] T. Cretegny, T. Dauxois, S. Ruffo, and A. Torcini, cond-mat/9709204 (unpublished).
[43] L. Brillouin, *Science and Information Theory* (Academic Press, New York, 1956).
[44] J. De Luca and A. Lichtenberg, Phys. Rev. E **66**, 026206 (2002).
[45] D. S. Saxon and R. A. Hunter, Philips Res. Rep. **4**, 81 (1949).
[46] J. M. Luttinger, Philips Res. Rep. **6**, 303 (1951).
[47] J. Hori, *Spectral Properties of Disordered Chains and Lattices* (Pergamon Press, Oxford, 1968).
[48] D. N. Payton and W. M. Visscher, Phys. Rev. **154**, 802 (1967).
[49] D. N. Payton and W. M. Visscher, Phys. Rev. **156**, 1032 (1967).